



## Neutronic Analysis of the European Sodium Fast Reactor: Part II - Burnup Results

Emil Fridman, Francisco Álvarez Velarde, Pablo Romojaro Otero, Haile Tsige-Tamirat, Antonio Jiménez Carrascosa, Nuria García Herranz, Franck Bernard, Robert Gregg, Una Davies, Jiri Krepel, et al.

### ► To cite this version:

Emil Fridman, Francisco Álvarez Velarde, Pablo Romojaro Otero, Haile Tsige-Tamirat, Antonio Jiménez Carrascosa, et al.. Neutronic Analysis of the European Sodium Fast Reactor: Part II - Burnup Results. Journal of Nuclear Engineering and Radiation Science, 2021, 8 (1), pp.11302. 10.1115/1.4048765 . irsn-04122521

**HAL Id: irsn-04122521**

**<https://irsn.hal.science/irsn-04122521>**

Submitted on 8 Jun 2023

**HAL** is a multi-disciplinary open access archive for the deposit and dissemination of scientific research documents, whether they are published or not. The documents may come from teaching and research institutions in France or abroad, or from public or private research centers.

L'archive ouverte pluridisciplinaire **HAL**, est destinée au dépôt et à la diffusion de documents scientifiques de niveau recherche, publiés ou non, émanant des établissements d'enseignement et de recherche français ou étrangers, des laboratoires publics ou privés.



Distributed under a Creative Commons Attribution 4.0 International License

## Neutronic analysis of the European Sodium Fast Reactor:

### Part II - burnup results

**Emil FRIDMAN**

Helmholtz-Zentrum Dresden-Rossendorf (HZDR)  
Bautzner Landstraße 400, 01328 Dresden, Germany  
[e.fridman@hzdr.de](mailto:e.fridman@hzdr.de)

**Francisco ÁLVAREZ VELARDE**

Centro de Investigaciones Energéticas, Medioambientales y Tecnológicas (CIEMAT)  
Av. Complutense, 40, 28040 Madrid, Spain  
[francisco.alvarez@ciemat.es](mailto:francisco.alvarez@ciemat.es)

**Pablo ROMOJARO OTERO**

CIEMAT (currently at SCK-CEN)  
Av. Complutense, 40, 28040 Madrid, Spain  
[Pablo.Romojaro@ciemat.es](mailto:Pablo.Romojaro@ciemat.es) ([Pablo.romojaro@sckcen.be](mailto:Pablo.romojaro@sckcen.be))

**Haile TSIGE-TAMIRAT**

European Commission / Joint Research Centre Petten  
Westerduinweg 3. 1755LE Petten  
[Haileyesus.TSIGE-TAMIRAT@ec.europa.eu](mailto:Haileyesus.TSIGE-TAMIRAT@ec.europa.eu)

**Antonio JIMÉNEZ CARRASCOSA**

Universidad Politécnica de Madrid (UPM)  
José Gutiérrez Abascal, 2, 28006 Madrid, Spain  
[antonio.icarrascosa@upm.es](mailto:antonio.icarrascosa@upm.es)

**Nuria GARCÍA HERRANZ**

Universidad Politécnica de Madrid (UPM)  
José Gutiérrez Abascal, 2, 28006 Madrid, Spain  
[nuria.garcia.herranz@upm.es](mailto:nuria.garcia.herranz@upm.es)

**Franck BERNARD**

Institut de Radioprotection et de Sûreté Nucléaire (IRSN)  
31 Avenue de la Division Leclerc, 92260 Fontenay-aux-Roses, France  
[franck.bernard@irsn.fr](mailto:franck.bernard@irsn.fr)

**Robert GREGG**

National Nuclear Laboratory (NNL)  
Chadwick House, Warrington WA3 6AE, UK  
[robert.wh.gregg@nnl.co.uk](mailto:robert.wh.gregg@nnl.co.uk)

**Una DAVIES**

University of Cambridge  
Trumpington St, Cambridge CB2 1PZ, UK  
[ud215@hermes.cam.ac.uk](mailto:ud215@hermes.cam.ac.uk)

**Jiri KREPEL**

Paul Scherrer Institut (PSI)  
5232 Villigen, Switzerland  
[jiri.krepel@psi.ch](mailto:jiri.krepel@psi.ch)

**Ben LINDLEY**

Jacobs  
Kings Point House, Queen Mother Square, Poundbury, Dorchester, DT1 3BW  
[Ben.Lindley@jacobs.com](mailto:Ben.Lindley@jacobs.com)

**Simone MASSARA**

EDF-R&D, EDF Lab Paris-Saclay (Currently at IAEA)  
7 Boulevard Gaspard Monge, 91120 Palaiseau, France  
[simone.massara@edf.fr](mailto:simone.massara@edf.fr) ([S.Massara@iaea.org](mailto:S.Massara@iaea.org))

**Sandra POUMEROULY**

EDF-R&D, EDF Lab Paris-Saclay  
7 Boulevard Gaspard Monge, 91120 Palaiseau, France  
[sandra.poumerouly@edf.fr](mailto:sandra.poumerouly@edf.fr)

**Enrico GIRARDI**

EDF-R&D, EDF Lab Paris-Saclay  
7 Boulevard Gaspard Monge, 91120 Palaiseau, France  
[enrico.girardi@edf.fr](mailto:enrico.girardi@edf.fr)

**Konstantin MIKITYUK**

Paul Scherrer Institut (PSI)  
5232 Villigen, Switzerland  
[konstantin.mikityuk@psi.ch](mailto:konstantin.mikityuk@psi.ch)

## Abstract

In the framework of the Horizon 2020 project ESFR-SMART (2017-2021), the European Sodium Fast Reactor (ESFR) core was updated through a safety-related modification and optimization of the core design from the earlier FP7 CP-ESFR project (2009-2013).

This study is dedicated to neutronic analyses of the improved ESFR core design. The conducted work is reported in two parts. Part I deals with the evaluation of the safety-related neutronic parameters of the fresh Beginning-of-Life (BOL) core carried out by 8 organizations using both continuous energy Monte Carlo and deterministic computer codes. In addition to the neutronics characterization of the core, a special emphasis was put on the calibration and verification of the computational tools involved in the analyses.

Part II is devoted to once-through and realistic batch-wise burnup calculations aiming at the establishing of the equilibrium core state, which will later serve as a basis for detailed safety analyses.

## 1. Introduction

The ESFR-SMART (European Sodium Fast Reactor Safety Measures Assessment and Research Tools) is a four-year collaborative project co-funded by the European Commission within the Euratom research and training programme [1]. The project has been launched to enhance further the safety of the commercial-size European Sodium Fast Reactor (ESFR) investigated within the earlier CP-ESFR project [2].

At the initial stage of the project, the modified ESFR core design was obtained through the two-step optimization procedure applied to the ESFR-CONF2 core from CP-ESFR. The new ESFR core design was established by optimizing neutronic, thermal-hydraulic, and fuel performance using multi-physics and multi-objective optimization. The core design modifications were aimed at improving the core map symmetry, optimizing the void effect, and facilitating the corium relocation toward the corium catcher. The corresponding activities are described in details in the current special issue on ESFR-SMART [3]. Some preliminary information is also available in [4].

The main objective of the current study is a neutronic characterization of the new ESFR core. The conducted work is reported in two parts. Part I focused on the evaluation of the safety-related neutronic parameters of the fresh core, which are used to calibrate and verify the computer codes used in the analyses [5]. Part II of the paper is devoted to once-through and realistic batch-wise burnup analysis aiming at the establishing of the equilibrium core loading configuration, which will later serve as a basis for detailed safety analyses.

Part II of the paper is structured as follows. Section 2 provides a brief overview of the initial ESFR core. Section 3 discusses once-through burnup calculations. Modeling assumptions and results of the batch-wise burnup analysis are presented in Section 4. Section 5 summarizes the paper.

## 2. A brief description of the initial ESFR-SMART core

This section provides a brief description of the new ESFR core and summarizes the major core parameters. The core description is similar to the one given in Part I of the paper [5] and provided here to facilitate the reading.

The radial core layout is shown in Figure 1. The core consists of inner fuel (IF) and outer fuel (OF) regions loaded with 216 and 288 fuel sub-assemblies (SA), respectively. In the initial core, the Pu content in both zones is equal to 17.99 wt%. Both regions are managed using a 6-batch fuel loading pattern. The core is controlled by 24 control and shutdown devices (CSD) and 12 dedicated shutdown devices (DSD). Compared to the ESFR-WH core, new corium discharge tubes (CDT) were introduced into several locations (31 in total) including the central position, the boundary between IF and OF regions, and the core periphery. The active core is surrounded by 3 rings of reflector SA, 2 rings of internal spent fuel storage positions, and 4 rings of shielding SA. A preliminary analysis, performed at CIEMAT, showed a negligible effect of the spent fuel storage and shielding on neutronics. Therefore, these regions were not considered in the neutronic analyses of the ESFR-SMART core. The core radius including reflector is about 3 m.

The axial layout and dimensions of the IF and OF SAs are presented in Figure 2. As in the ESFR-CONF2 core from the CP-ESFR project, a large sodium plenum followed by a neutron absorber was introduced above the active core. In addition, the heights of the fissile regions were reduced and fertile and steel blankets were introduced below. A single fissile enrichment was adopted for both IF and OF regions. In order to decrease the sodium void effect and improve the radial

Journal of Nuclear Engineering and Radiation Science

power uniformity, the height of the IF fissile region was further reduced. At room temperature, the active core height is 1 m. The height of the blanket in IF and OF zones is 25 and 5 cm respectively. The height of the sodium plenum is 60 cm.

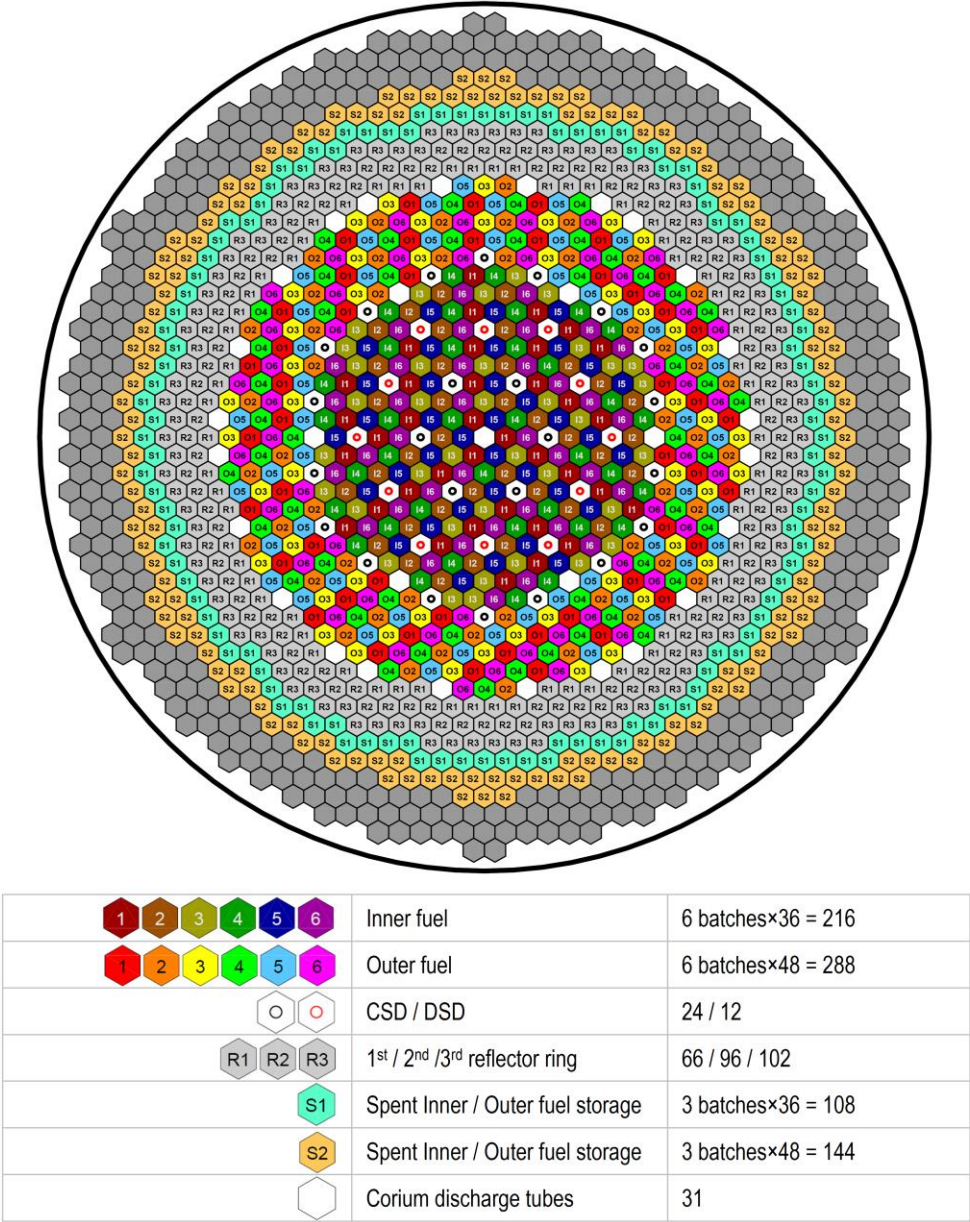


Fig. 1 Radial core layout

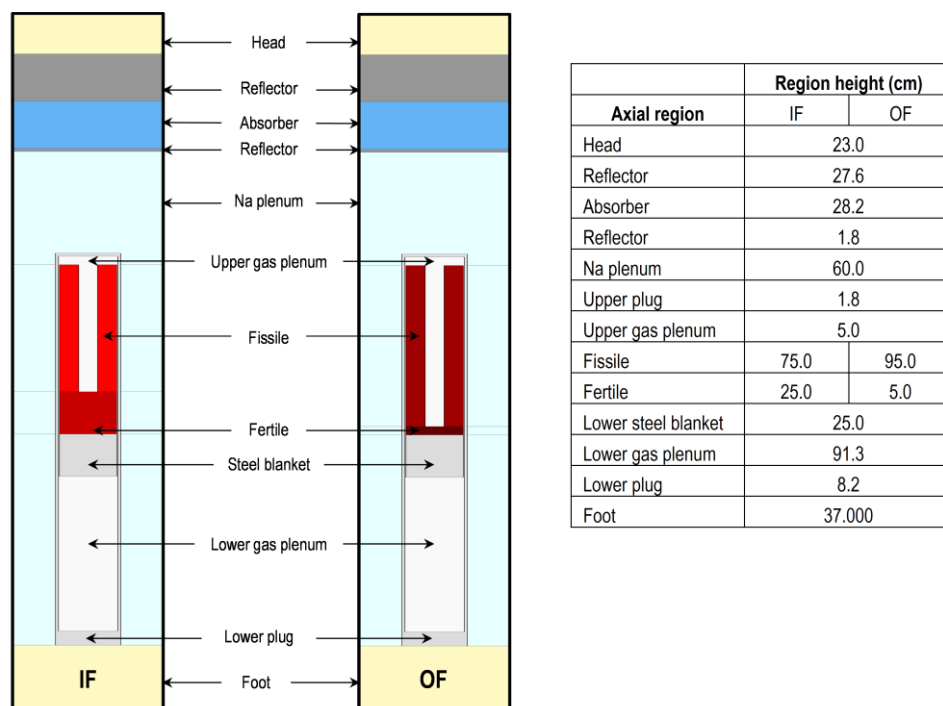


Fig. 2 Axial core layout and dimensions (as fabricated)

### 3. Once-through burnup calculations

#### 3.1 Modeling assumptions

The initial core neutronic calculations reported in [5] were followed by the once-through burnup analysis. The calculations were carried out by 7 organizations presented in Table 1. Four institutions, namely HZDR, CIEMAT, IRSN, and UPM, utilized Monte Carlo (MC) based burnup codes. The MC Serpent, applied by HZDR, includes a built-in decay and depletion solver [6]. UPM performed calculations with KENO-VI which is coupled with ORIGEN depletion solver within the SCALE code system [7]. CIEMAT and IRSN used the EVOLCODE 2.0 [8] and VESTA 2.2.0 [9] codes which couple MCNP with the depletion solvers ACAB [10] and PHOENIX, respectively. The deterministic results were produced by NNL and Cambridge University using WIMS [11]. For this calculation, WIMS-CACTUS (method of characteristics) was used to calculate 172 group cross sections for the different lattices present in the core. WIMS-MERLIN, an SP3 (Simplified P3 transport) method, was then used to solve the flux distribution across the whole core using a HEX-Z model. Deterministic results were also produced by PSI as well as EDF using ERANOS/VARIANT [12].

Table 1. Participants and codes used for once-through burnup calculations.

Organization	Code	Nuclear data library
HZDR	Serpent 2.1.29	JEFF-3.1
CIEMAT	EVOLCODE 2.0 (MCNP6.1.1b + ACAB) [8,10]	JEFF-3.1
IRSN	VESTA 2.2.0 (MCNP6.1.1b + PHOENIX 2.2.0) [9]	JEFF-3.1
UPM	SCALE6.2.3 (KENO-VI + ORIGEN) [7]	JEFF-3.1
NNL/Cambridge	WIMS11 [11]	JEFF 3.1.2
PSI	ERANOS/VARIANT [12]	JEFF-3.1
EDF	ERANOS/VARIANT [12]	JEFF-3.1

The calculations were performed for a total of 2100 effective full power days (EFPD) assuming all-fresh fuel with identical Pu content in all 6 fuel batches at beginning of life (BOL). Fuel SAs reloading and reshuffling was not considered. During the entire campaign, all control devices were withdrawn to a parking position at the top of the upper gas plenum. The core power was 3600 MW<sub>th</sub>.

Concerning the reference axial discretization, the inner core was subdivided into 8 burnable regions (3 fertile + 5 fissile) while the outer core was subdivided into 6 burnable regions (1 fertile + 5 fissile). It should be noted that the WIMS calculations were performed using 20 axial zones.

In radial directions, two options were considered:

- Option 1: Batch-wise discretization with 6 radial burnable regions in IF and OF. This option assumes that all fuel SAs, belonging to a certain batch, form a single burnable region.
- Option 2: SA-wise burnup with 216 radial burnable regions in IF and 288 radial burnable regions in OF.

Option 1 and Option 2 lead to a total of 84 and 3456 burnable regions respectively. The latter can be prohibitively expensive for MC-based burnup codes. Therefore, the former was adopted as a reference discretization option. The evaluated parameters include burnup dependent quantities such as core reactivity and isotopic composition as well as axial power profiles.

### 3.2 Results: once-through burnup calculations

#### 3.2.1 Core reactivity

The burnup dependent core reactivity is plotted in Figure 3 and the differences relative to the Serpent reference are presented in Figure 4. For the MC codes, the reported standard deviation of reactivity in pcm units is as follows: HZDR (Serpent) - 4, CIEMAT (EVOLCODE) - 13, IRSN (VESTA) - 13, UPM (SCALE) - 10. The Serpent (HZDR), EVOLCODE (CIEMAT), and VESTA (IRSN) results show a good agreement over entire burnup campaign with a maximum discrepancy of 250 pcm. KENO (UPM) agrees very well with Serpent at BOL. However, the differences are monotonically increasing with burnup and reaching 785 pcm at end of life (EOL), which can be partially attributed to the disabling of the probability tables in the unresolved resonance region. A more detailed discussion on the effect of unresolved resonances can be found in the previous studies by the authors [5,13]. The deviation between Serpent and WIMS does not exceed 170 pcm. As compared to Serpent, ERANOS underestimates the reactivity at BOL and predicts higher values at EOL. It is worth noting that the reactivity predicted with ERANOS by PSI and EDF are in very good agreement on the first half of the irradiation (<1000 EFPD), but differs by 200 pcm at EOL.

#### 3.2.2 Isotopic composition

The evolution of isotopic composition<sup>1</sup> with burnup, for calculations performed with the Serpent code, is presented in Figures 5-6. During the irradiation campaign, the total Pu content in the fissile regions of IF and OF (respectively denoted as IF-FI and OF-FI) remains approximately constant with a slight increase in the Pu-239 amount and a moderate reduction in the Pu-241 amount (Figure 5). The amount of Am-241 increases by about 60% towards EOL.

---

<sup>1</sup> Expressed as atomic number densities (ND)

In the fertile regions (IF-FE for region IF, OF-FE for region OF), there is a steep increase in the Pu-239 content, which constitutes about 89% of the total Pu amount at EOL (Figure 6). The share of Pu-240 reaches 10% and other Pu isotopes constitute less than 1% of the total Pu.

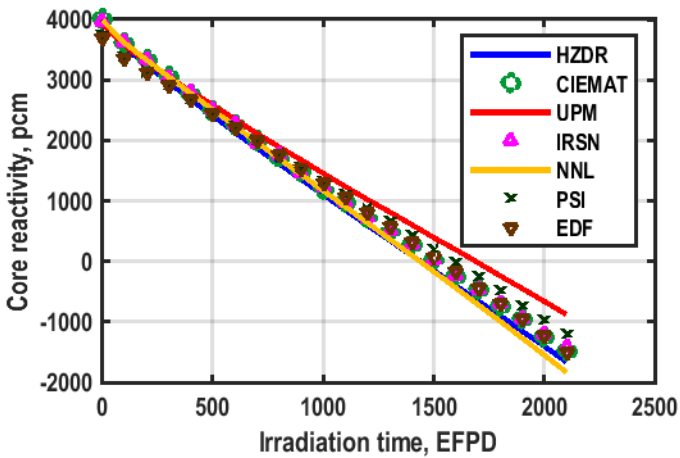


Fig. 3 Core reactivity as a function of irradiation time

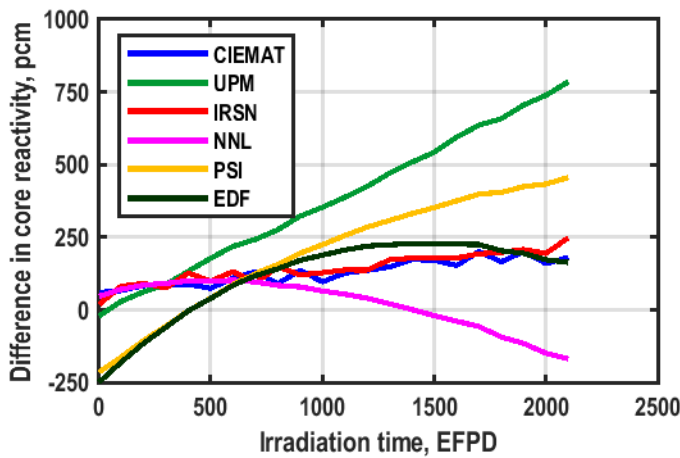


Fig. 4 Differences in core reactivity vs. Serpent

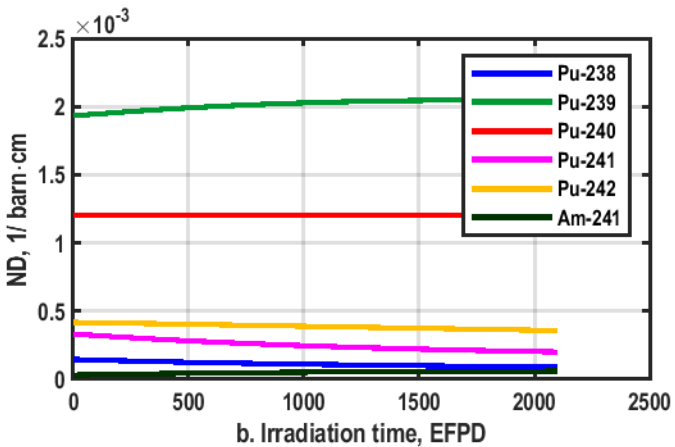
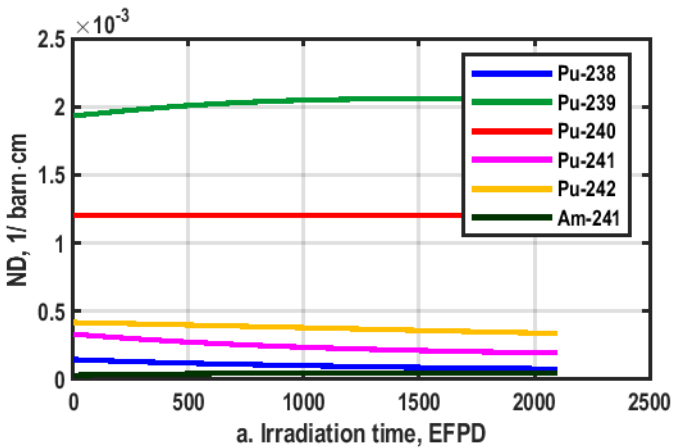


Fig. 5 Evolution of isotopic composition in the fissile zones, Serpent result: a. averaged over IF-FI; b. averaged over OF-FI.

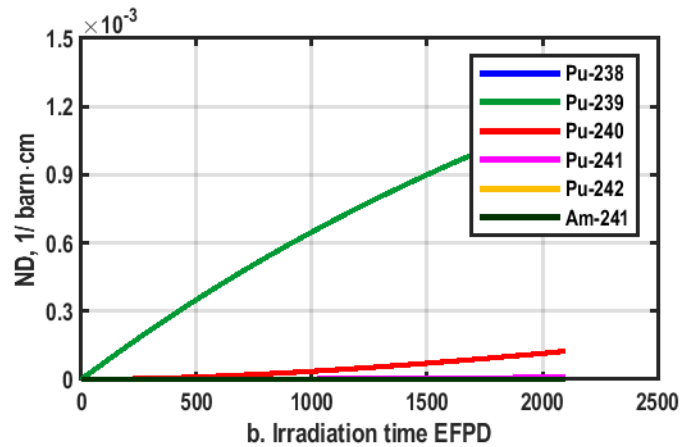
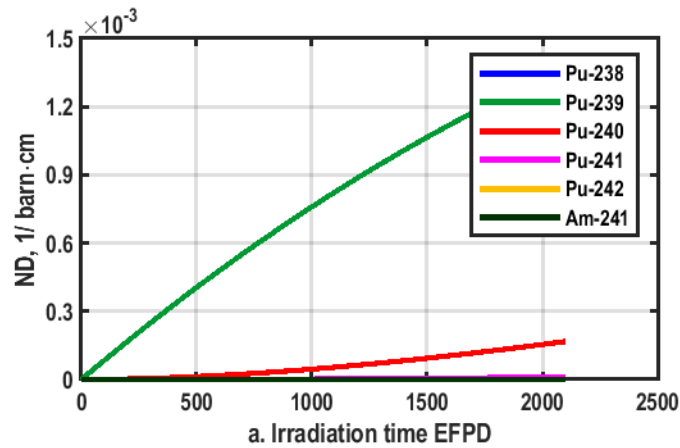


Fig. 6 Evolution of isotopic composition in the fertile zones, Serpent result: a. averaged over IF-FE; b. averaged over OF-FE.

The EOL isotopic compositions of the inner and outer fissile zones predicted by the different codes show generally good agreement (Figure 7-8). The EOL amount of Pu-239 to 242 and Am-241 predicted by Serpent agree within 0.4% with VESTA (IRSN) and KENO (UPM). The deterministic results have a slightly higher discrepancy of about 1.3% for Pu-239 to



242 and 2.1% for Am-241. EVOLCODE (CIEMAT) noticeably underpredicts the amount of Pu-241 and, consequently, the amount of Am-241.

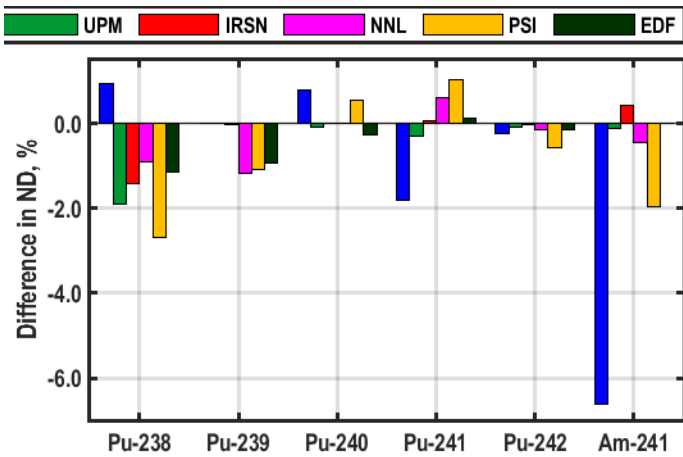


Fig. 7 Differences in isotopic composition of IF-FI at EOL vs. Serpent

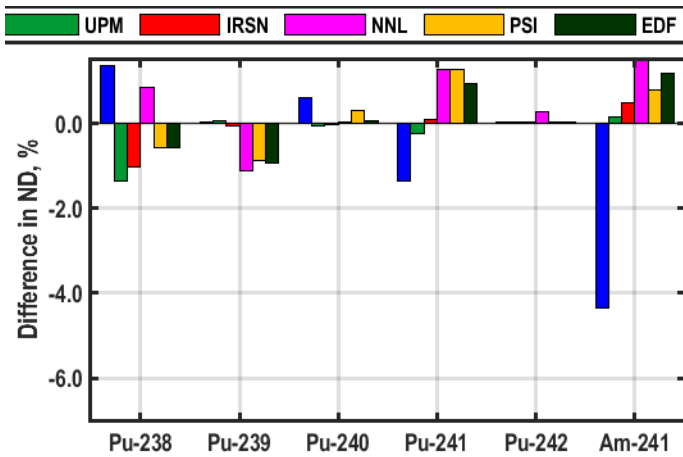


Fig. 8 Differences in isotopic composition of OF-FI at EOL vs. Serpent.

The EOL isotopic compositions of the fertile zones exhibit significantly higher spread as shown in Figures 9-10 for the inner and outer regions, respectively. Compared to the reference Serpent solution, the major differences were found in the amounts of Pu-238, 241, 242 and Am-241 calculated by the deterministic codes. The relative differences are high but correspond to small absolute quantities. The corresponding results obtained with the MC-based depletion codes (CIEMAT, UPM, and IRSN) show much lower deviation from the reference. The amounts of the dominant Pu isotopes (i.e. Pu-239 and Pu-240), estimated by the MC codes, agree within less than 3% while the deterministic results deviate by more than 6% from those from Serpent.

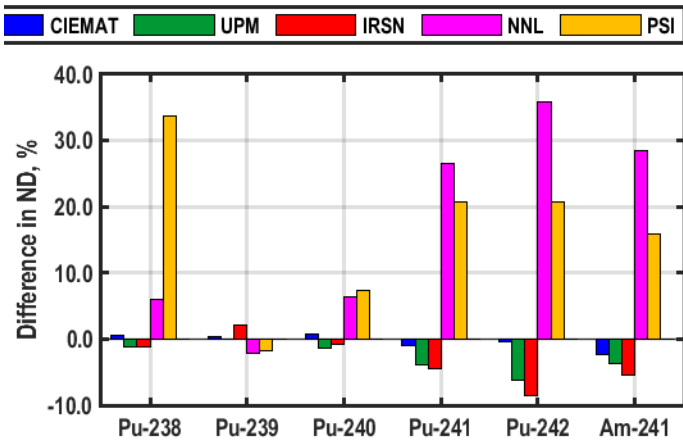


Fig. 9 Differences in isotopic composition of IF-FE at EOL vs. Serpent

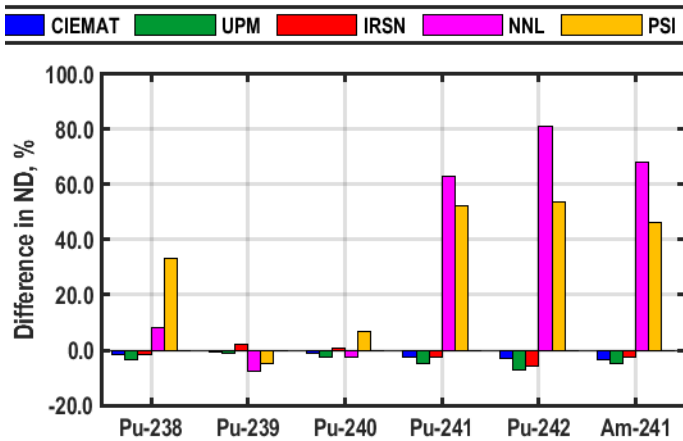


Fig. 10 Differences in isotopic composition of OF-FE at EOL vs. Serpent

### 3.2.3 Axial power profiles

Region-averaged axial power profiles at BOL and EOL are depicted in Figure 11. Towards EOL, there is a clear shift in power profiles in both IF and OF regions due to Pu breeding in the lower blankets as shown in Fig. 6. The power share between blanket and fuel regions increased from 1.3% to 12.9% and from 0.3% to 2.0% for IF and OF, respectively. The corresponding results provided by three organizations, namely HZDR, CIEMAT, and NNL, are in a very good agreement.

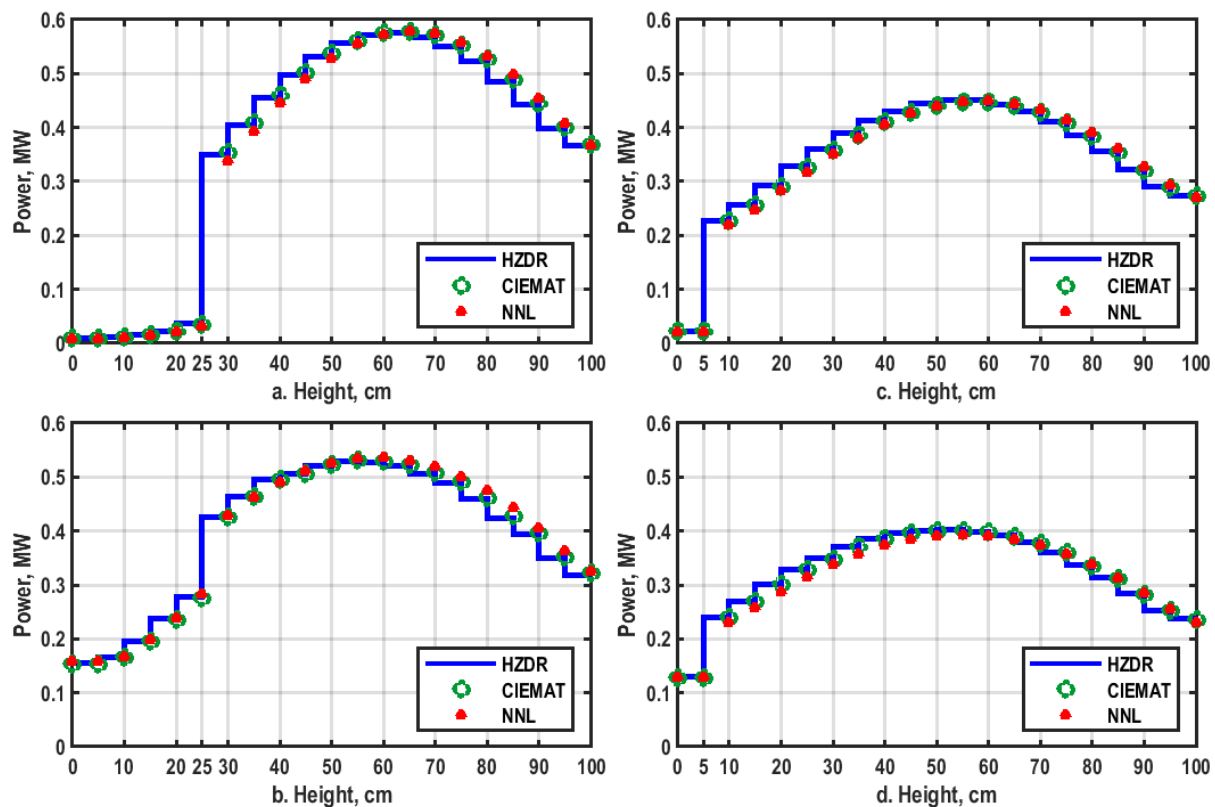


Fig. 11 Region-averaged axial power profiles: a. IF region at BOL; b. IF region at EOL; c. OF region at BOL; d. OF region at EOL.

#### 4. Multi-batch burnup calculations

##### 4.1 Modelling assumptions

The once-through burnup analysis, reported in Section 3, was performed in a “single-batch” mode starting with the all-fresh fuel with identical Pu content in all SAs. However, the new ESFR core was designed to be operated in a 6-batch mode. This implies that after a certain period of time, designated as a “fuel cycle”, one fuel batch in both fuel regions is discharged and replaced by fresh fuel SAs. The objective of the current study is to achieve the equilibrium 6-batch core state by performing multi-batch burnup calculations including the reloading of the fuel batches. The following modelling assumptions were made:

- The total in-core residence time of a single batch was fixed to 2172 EFPD.
- The fuel cycle length was fixed to 362 EFPD (i.e. 1/6th of the total fuel in-core residence time).
- Every fuel batch comprises 36 inner and 48 outer SAs (i.e. 1/6th of the total number of SAs).
- The fuel SAs were loaded according to the 6-batch loading scheme shown in Figure 1.
- The fuel SAs are not shuffled i.e. keep their positions for the entire in-core residence time.
- The equilibrium core was established through the simulation of the 3 full in-core residence periods (i.e. 18 successive fuel cycles).
- The fuel SAs were managed using the re-loading scheme shown in Table 2.
- All control devices are at the parking position.

- The axial and radial core discretization was identical to “Option 1” used for the once-through burnup calculation (see Section 3.1).

Table 2. Fuel re-loading scheme for the 6-batch core showing a number of accumulated in-core residence cycles for every batch and fuel cycle. The discharged batch is shaded by green.

Batch	Cycle 1		Cycle 2		Cycle 3		Cycle 4		Cycle 5		Cycle 6	
	BOC1*	EOC1	BOC2	EOC2	BOC3	EOC3	BOC4	EOC4	BOC5	EOC5	BOC6	EOC6
1	Fresh	1	1	2	2	3	3	4	4	5	5	6
2	1	2	2	3	3	4	4	5	5	6	Fresh	1
3	2	3	3	4	4	5	5	6	Fresh	1	1	2
4	3	4	4	5	5	6	Fresh	1	1	2	2	3
5	4	5	5	6	Fresh	1	1	2	2	3	3	4
6	5	6	Fresh	1	1	2	2	3	3	4	4	5

\*BOC = beginning of cycle, EOC = end of cycle

The evaluated parameters include cycle-wise core reactivity and several parameters characterizing the core at the End of Equilibrium Cycle (EOEC) state such as radial power distribution, batch-wise axial power distribution, and batch-wise axial burnup profiles. The multi-batch burnup calculations were performed by HZDR using Serpent, by PSI using ERANOS, and by NNL using WIMS. All organizations employed JEFF3.1 nuclear data library.

## 4.2 Results: Multi-batch burnup calculations

### 4.2.1 Cycle-wise core reactivity

The cycle-wise core reactivity calculated by Serpent (HZDR) and ERANOS (PSI) for 2 from 3 consecutive full in-core residence periods is presented in Figure 12 while omitting the results of the first transitional period. It should be noted that in the WIMS (NNL) case only 2 full in-core residence periods were modeled. Therefore, the cycle-wise core reactivity, calculated by WIMS, is plotted for the second period only (Figure 12). Although all fuel cycles were modelled sequentially, the starting point of every full in-core period in the plot was set to 0 EFPD for comparison purposes.

In Serpent case, the cycle-wise reactivity of the two presented in-core residence periods is very close and agrees within less than 20 pcm, thus, indicating the equilibrium core state. The BOC reactivity is around 1400 pcm, which is significantly lower than the BOL reactivity of about 4000 pcm in the once-through case. For both simulated periods, the BOC reactivity slightly varies from cycle to cycle. Since the fuel SAs are not shuffled within the core, this can be explained by a somewhat different reactivity worth of the different fuel batches. In all cycles, there is sufficient EOC reactivity margin of around 500 pcm.

The ERANOS (PSI) results are close to those of Serpent and exhibit a similar cycle-wise behavior. However, there is somewhat higher discrepancy in reactivity between two residence periods. In the ERANOS case, the cross-sections are recalculated according to the actual burnup state only after every 6 batches, at the end of the 6 batch period. Therefore, achieving the equilibrium state may require a higher number of 6 batch period calculations.

The cycle-wise core reactivity predicted by WIMS (NNL) is systematically higher than that of Serpent, although the qualitative behavior is quite comparable. The discrepancies between the codes can be partially attributed to the differences in the axial meshing. In WIMS, much finer nodalization was applied as compared to Serpent.

It is worth mentioning that the behavior of the reactivity curve can be quite sensitive to the nuclear data library applied. As an example, a comparison of cycle-wise reactivity obtained by Serpent with two different cross sections sets (JEFF-3.1 and ENDF/B-VII.0) is shown in Figure 13. It is worth mentioning that the reactivity margin at EOC is about 400 pcm for JEFF-3.1 and reduces to about 250 pcm with ENDF/B-VII.0, which may question the robustness of the hypothesis of a 2172 EFPD cycle length.

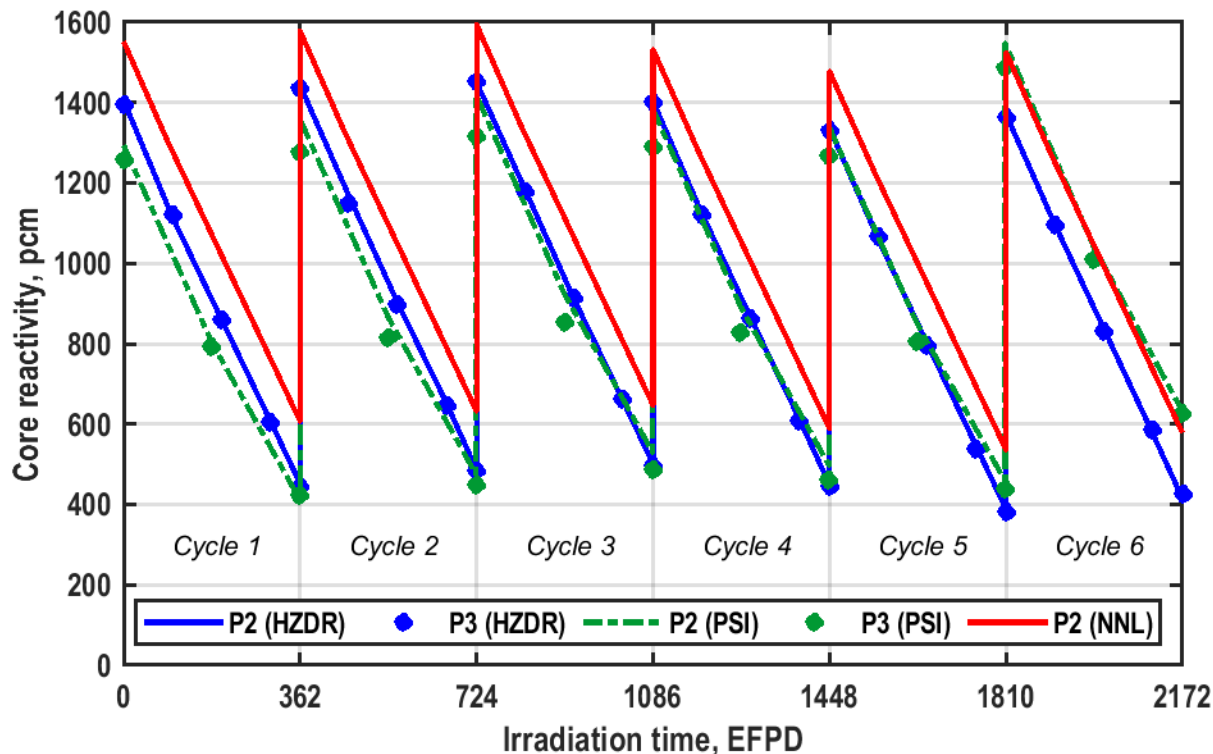


Fig. 12 Cycle-wise core reactivity for 2 consecutive full in-core residence periods

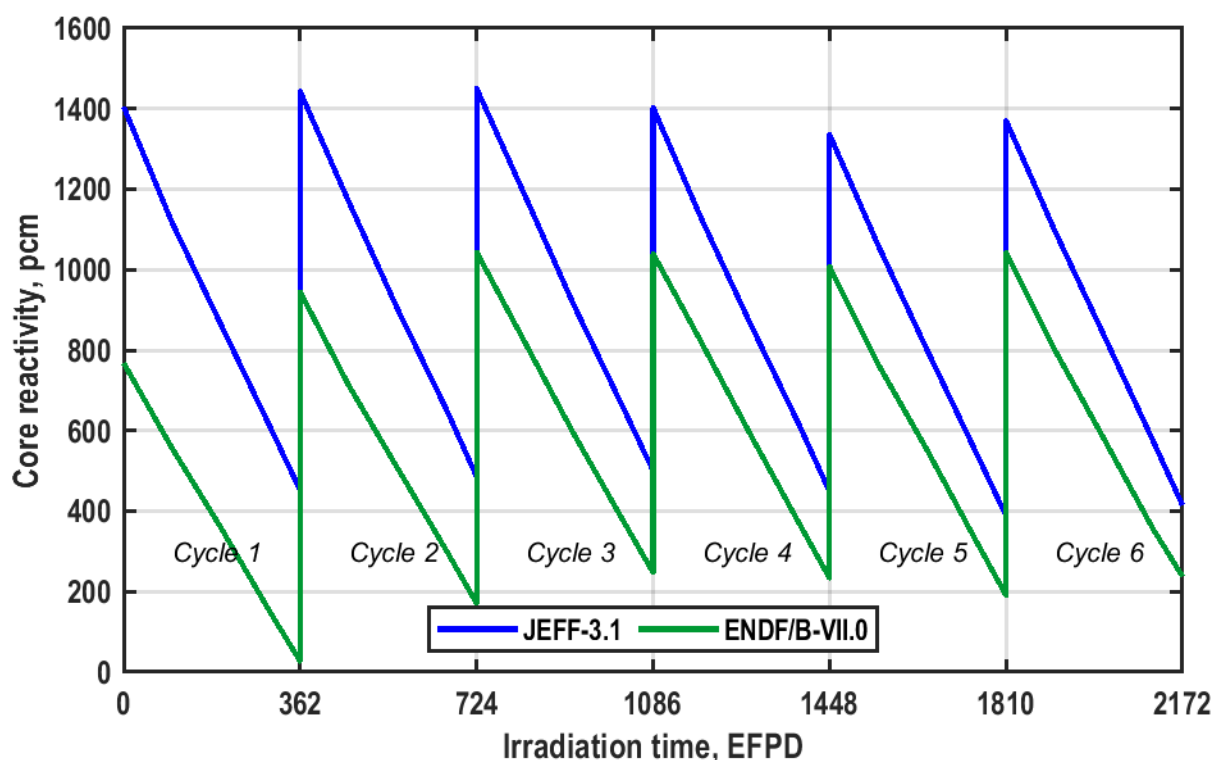


Fig. 13 Cycle-wise core reactivity obtained with two different cross sections sets computed with Serpent

#### 4.2.2 Initial characterization of the EOEC core

Since the cycle-wise core behavior is approximately identical, the EOC state of the 3<sup>rd</sup> in-core residence period was considered as the EOEC state. The corresponding average core burnup is about 58.2 MWd/kg. In this section the following parameters, are reported: radial power distribution (Figure 14), batch-wise axial power distribution (Figure 15 and Figure 16), and batch-wise axial burnup profiles (Figure 17 and Figure 18).

This core state will be used in the follow-up studies for further more detailed analysis. For example, the EOEC core will be studied to assess a bunch of the safety relevant parameters such as a detailed spatial distribution of Doppler constants and sodium void reactivity, decay heat distribution, and other safety-related parameters. The EOEC core will be also analyzed using coupled core thermal hydraulics and neutronics simulations. The obtained EOEC core state will also serve as a basis for the modeling of the system behavior in selected accident scenarios (both protected and unprotected).

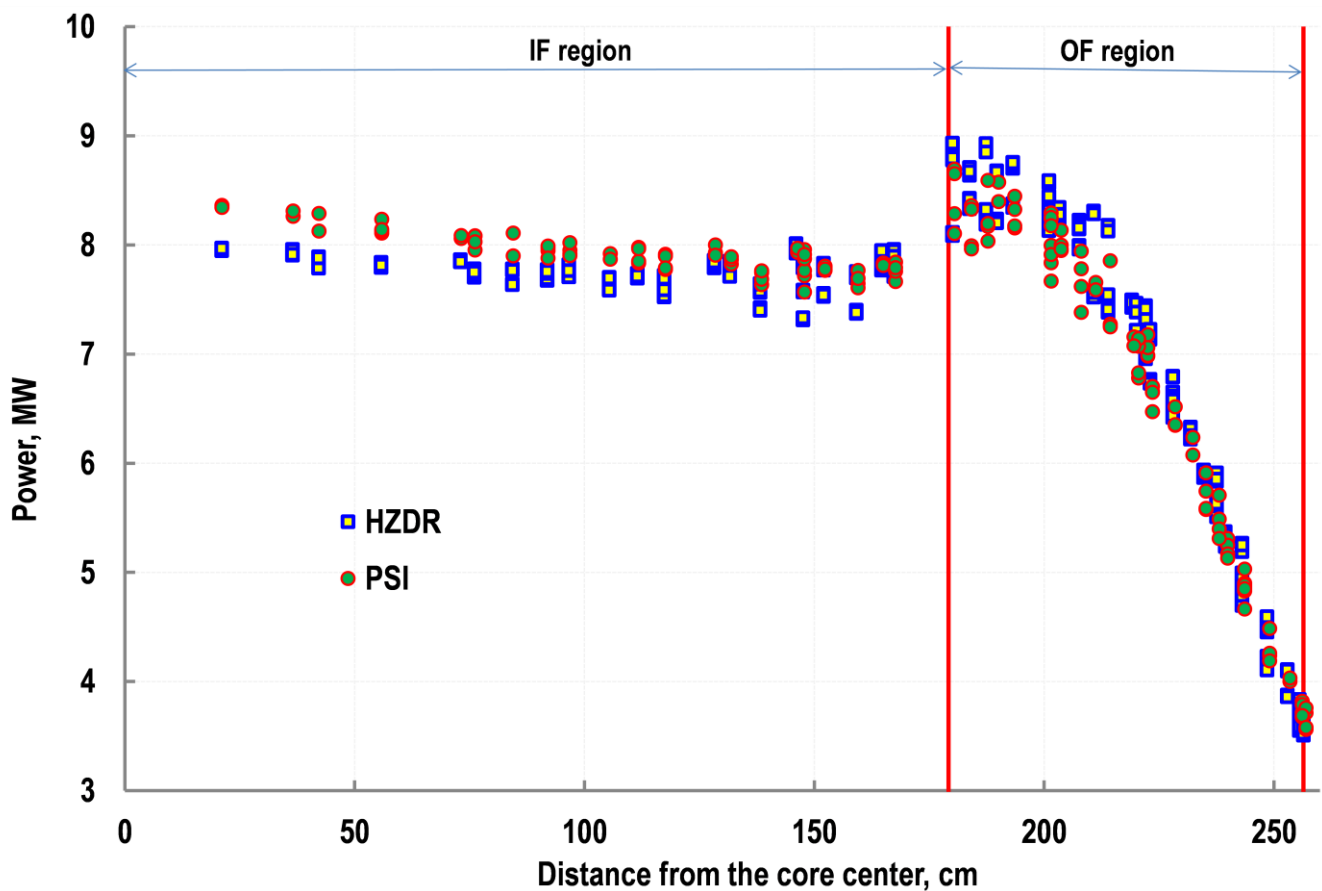


Fig. 14 Radial power profile at EOEC

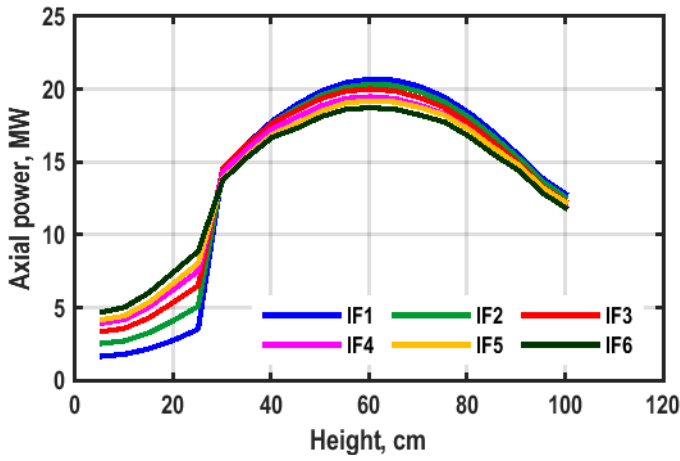


Fig. 15 IF batch-wise axial power profiles at EOEC computed by Serpent

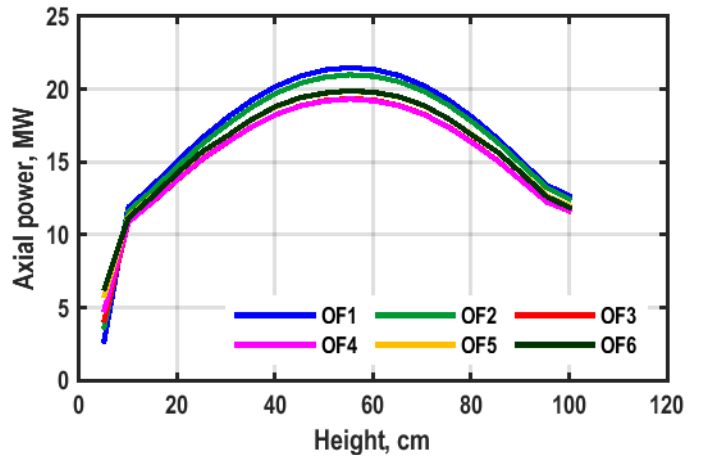


Fig. 16 OF batch-wise axial power profiles at EOEC computed by Serpent

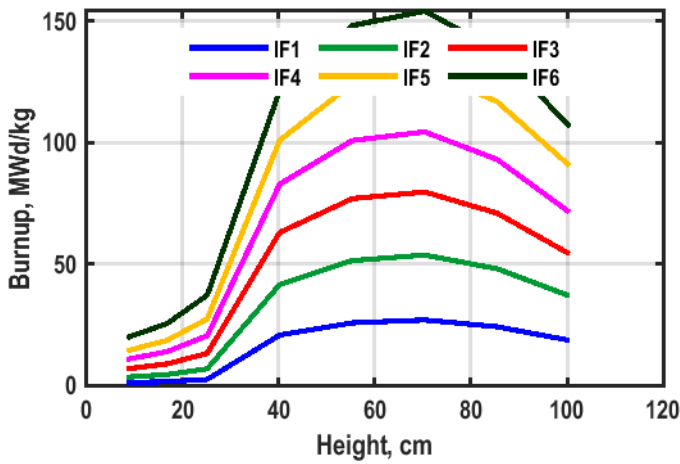


Fig. 17 IF batch-wise axial burnup profiles at EOEC computed by Serpent

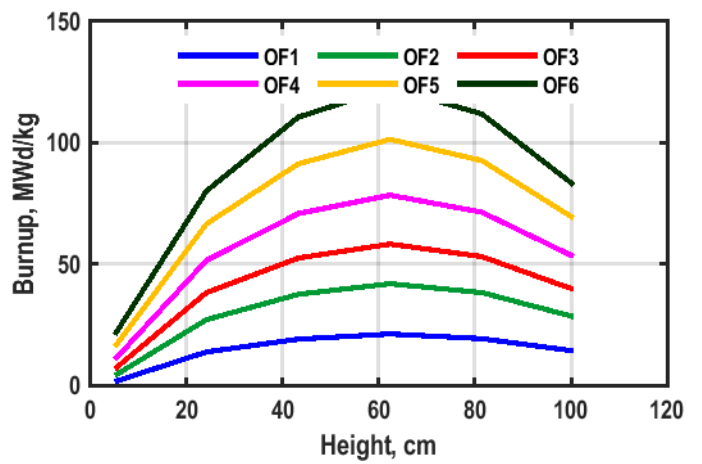


Fig. 18 OF batch-wise axial burnup profiles at EOEC computed by Serpent

#### 4.2.3 Breeding performance in the multi-batch operation

The ESRF-SMART core is designed as an iso-breeder. Accordingly, the mass of fissile nuclides should stay constant during irradiation or just slightly increase. For checking of this feature the plutonium balance in the inner and outer core and in the fissile and fertile zone was assessed. The outcome is illustrated by Fig. 19 and 20. The plutonium vector is constant. It does not change throughout the 6 batch cycle (See Fig 19). There are just mild oscillation caused by the small difference between the initial plutonium composition and discharged plutonium composition.

The absolute mass of Pu is increasing during the irradiation (see Fig. 20). During one batch roughly 50 kg of Pu are bred. It corresponds to a Pu mass increase of 0.4% in one year. Nonetheless, the Pu production is strongly distributed in the core. The inner and outer fissile zones act as a slight burner. The Pu mass in these zones is decreasing. During one batch irradiation it is up to 10 kg for the entire core. The smaller blanket in the outer zone has negligible impact; however, it is producing Pu. The major contribution comes from the inner blanket zone. According to the burnup level, each of the assembly groups produces from 12 to 22 kg of Pu in the blanket per year. The production depends on the assembly burnup state, since the fission source is increasing in the blanket zone with the burnup. In general, the breeding performance fulfills the expectation.

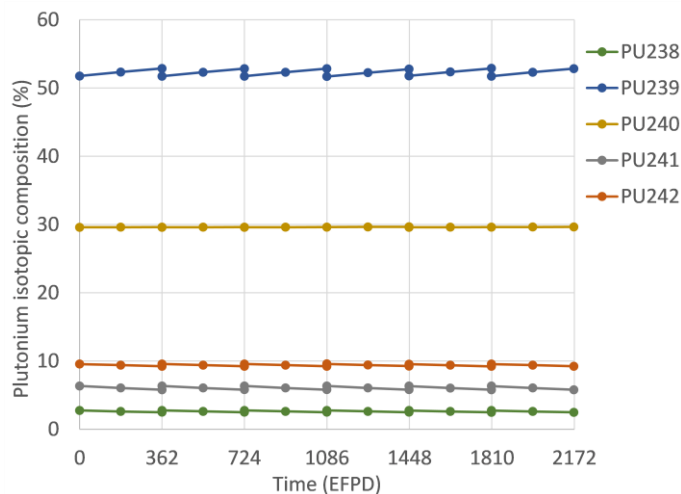


Fig. 19 Plutonium isotopic composition evolution during the batch-wise operation calculated by ERANOS code.

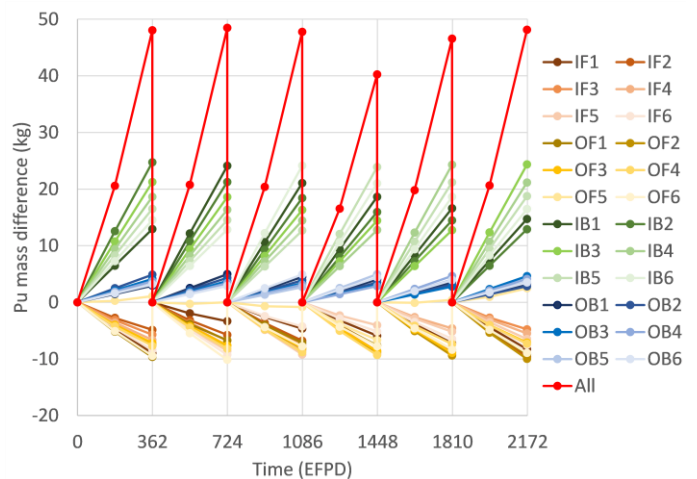


Fig. 20 Evolution of Pu mass difference during the batch-wise operation calculated by ERANOS code

## 5. Summary and conclusions

Part II of the paper reported on the burnup analysis of the newly proposed ESFR core. Initially, once-through full core burnup calculations were performed by 7 organizations using MC-based and deterministic depletion codes. The reported results, including temporal evolution of the core reactivity and isotopic compositions, show generally acceptable mutual agreement.

The once-through calculations were followed by the more realistic multi-batch burnup analysis performed by 3 organizations. The main objective was the establishing of the equilibrium core state. The desired equilibrium 6-batch core was obtained through the simulation of up to 18 successive fuel cycles, equivalent to the 3 full in-core residence periods. The fuel cycle length was kept constant at 362 EFPD. As compared to once-through cases, the BOC reactivity in the multi-batch scenario significantly reduced from about 4000 pcm to around 1400 pcm. The BOC reactivity slightly varies from cycle to cycle due to the constant location of fuel SAs within the core. The analyzed ESFR core acts as iso-breeder with the absolute increase of Pu mass equal to 0.4%/year. It should be pointed out that the Pu production is strongly distributed in the core. The inner and outer fissile zones act as slight burners while the inner blanket zone acts as a major Pu breeder.

Since in multi-batch scenario, the cycle-to-cycle behavior of the core is approximately identical, the EOC state of the 3rd in-core residence period was considered as the EOEC state. The corresponding average core burnup is about 58.2 MWd/kg. The selected EOEC core state, obtained in the current study, will be used as a basis for the follow-up more detailed analyses. This includes, for example, an assessment of the safety relevant parameters such as a detailed spatial distribution of Doppler constants and sodium void reactivity, decay heat distribution, and other safety-related parameters. The steady state performance of the EOEC core will be analyzed using coupled core thermal hydraulics and neutronics simulations. The obtained EOEC core state will be also used for the modeling of the system behavior in selected accident scenarios. The summary of these activities will be reported in the follow-up papers in the current Special Issue.

## Funding

The research leading to these results has received funding from the Euratom research and training programme 2014-2018 under Grant Agreement Number 754501 (ESFR-SMART)

## Acronyms and Abbreviations

BOL	=	Beginning Of Life
CDT	=	Corium Discharge Tubes
CSD	=	Control And Shutdown Devices
DSD	=	Dedicated Shutdown Devices
EFPD	=	Effective Full Power Days
EOEC	=	End Of Equilibrium Cycle
EOL	=	End Of Life
ESFR	=	European Sodium Fast Reactor
ESFR-SMART	=	European Sodium Fast Reactor Safety Measures Assessment and Research Tools
FE	=	Fertile
FI	=	Fissile
IF	=	Inner Fuel
MC	=	Monte Carlo
ND	=	Number Density
OF	=	Outer Fuel
pcm	=	per cent mille
SA	=	Sub-Assembly

## References

- [1] K. Mikityuk, E. Girardi, J. Krepel, E. Bubelis, E. Fridman, A. Rineiski, N. Girault, F. Payot, L. Buligins, G. Gerbeth, N. Chauvin, C. Latge, J.-C. Garnier, 2017. ESFR-SMART: new Horizon-2020 project on SFR safety, in proc. IAEA FR2017.
- [2] G.L. Fiorini, A. Vasile, 2011. European Commission – 7th Framework Programme: The Collaborative Project on European Sodium Fast Reactor (CP ESFR), Nuclear Engineering and Design. Vol. 241, pp. 3461–3469. <https://doi.org/10.1016/j.nucengdes.2011.01.052>.
- [3] A. Rineiski, C. Meriot, M. Marchetti, J. Krepel, H. Tsige-Tamirat, F. Alvarez, E. Girardi, K. Mikityuk, 2020. New core safety measures and their preliminary assessment in the ESFR-SMART project, Journal of Nuclear Engineering and Radiation Science. Vol. submitted,.
- [4] A. Rineiski, C. Meriot, M. Marchetti, J. Krepel, 2018. Core Safety Measures in ESFR-SMART, in proc. PHYSOR 2018.
- [5] E. Fridman, F. Álvarez-Velarde, P. Romojaro-Otero, H. Tsige-Tamirat, A. Jiménez-Carrascosa, N. García-Herranz, F. Bernard, R. Gregg, J. Krepel, S. Massara, S. Poumerouly, E. Girardi, K. Mikityuk, 2020. Neutronic analysis of the European Sodium Fast Reactor: Part I - fresh core results, Journal of Nuclear Engineering and Radiation Science. Vol. submitted,.
- [6] M. Pusa, J. Leppänen, 2010. Computing the Matrix Exponential in Burnup Calculations, Nuclear Science and Engineering. Vol. 164, pp. 140–150. <https://doi.org/10.13182/NSE09-14>.



- [7] B.T. Rearden, M.A. Jessee, 2017. SCALE Code System, <https://doi.org/10.2172/1408010>.
- [8] F. Álvarez-Velarde, E.M. González-Romero, I.M. Rodríguez, 2014. Validation of the burn-up code EVOLCODE 2.0 with PWR experimental data and with a Sensitivity/Uncertainty analysis, *Annals of Nuclear Energy*. Vol. 73, pp. 175–188. <https://doi.org/10.1016/J.ANUCENE.2014.06.049>.
- [9] W. Haeck, B. Cochet, L. Aguiar, 2012. Monte Carlo depletion calculations using VESTA 2.1 new features and perspectives, in *proc. PHYSOR 2012*.
- [10] J. Sanz, O. Cabellos, N. García-Herranz, 2008. ACAB-2008: Activation Code V2008, <https://doi.org/NEA-1839>.
- [11] B. Lindley, G. Hosking, P. Smith, D. Powney, B. Tollit, T. Fry, R. Perry, T. Ware, C. Murphy, C. Grove, M. Thomas, K. Hesketh, D. Kotlyar, 2017. Developments within the WIMS Reactor Physics Code for Whole Core Calculations, in *proc. M&C2017*.
- [12] J.M. Ruggieri, J. Tommasi, J.F. Lebrat, C. Suteau, D. Plisson-Rieunier, C. De Saint Jean, G. Rimpault, J.C. Sublet, 2006. ERANOS 2.1: International code system for GEN IV fast reactor analysis, in *proc. ICAPP 2006*.
- [13] A. Jiménez-Carrascosa, E. Fridman, N. García-Herranz, F. Alvarez-Velarde, P. Romojaro, F. Bostelmann, 2019. About the impact of the Unresolved Resonance Region in Monte Carlo simulations of Sodium Fast Reactors, in *proc. ICAPP 2019*. <https://doi.org/10.5281/zenodo.3324476>.